ADVANCES IN ATMOSPHERIC SCIENCES, VOL. 31, JULY 2014, 916–925

Boreal Winter Rainfall Anomaly over the Tropical Indo-Pacific and Its Effect on Northern Hemisphere Atmospheric Circulation in CMIP5 Models

WANG Hai* and LIU Qinyu

Physical Oceanography Laboratory/Qingdao Collaborative Innovation Center of Marine Science and Technology, Ocean–Atmosphere Interaction and Climate Laboratory, Ocean University of China, Qingdao 266100

(Received 23 August 2013; revised 11 December 2013; accepted 14 December 2013)

ABSTRACT

Experimental outputs of 11 Atmospheric Model Intercomparison Project (AMIP) models from phase 5 of the Coupled Model Intercomparison Project (CMIP5) are analyzed to assess the atmospheric circulation anomaly over Northern Hemisphere induced by the anomalous rainfall over tropical Pacific and Indian Ocean during boreal winter. The analysis shows that the main features of the interannual variation of tropical rainfall anomalies, especially over the Central Pacific (CP) (5°S–5°N, 175°E–135°W) and Indo-western Pacific (IWP) (20°S–20°N, 110°–150°E) are well captured in all the CMIP5/AMIP models. For the IWP and western Indian Ocean (WIO) (10°S–10°N, 45°–75°E), the anomalous rainfall is weaker in the 11 CMIP5/AMIP models than in the observation. During El Niño/La Niña mature phases in boreal winter, consistent with observations, there are geopotential height anomalies known as the Pacific North American (PNA) pattern and Indo-western Pacific and East Asia (IWPEA) pattern in the upper troposphere, and the northwestern Pacific anticyclone (cyclone) (NWPA) in the lower troposphere in the models. Comparison between the models and observations shows that the ability to simulate the PNA and NWPA pattern depends on the ability to simulate the anomalous rainfall over the CP, while the ability to simulate the IWPEA pattern is related to the ability to simulate the rainfall anomaly in the IWP and WIO, as the SST anomaly is same in AMIP experiments. It is found that the tropical rainfall anomaly is important in modeling the impact of the tropical Indo-Pacific Ocean on the extratropical atmospheric circulation anomaly.

Key words: Atmospheric Model Intercomparison Project, tropical Indo-Pacific rainfall, Northern Hemisphere atmospheric circulation anomaly, boreal winter, teleconnection pattern

Citation: Wang, H., and Q. Y. Liu, 2014: Boreal winter rainfall anomaly over the tropical Indo-Pacific and its effect on Northern Hemisphere atmospheric circulation in CMIP5 models. *Adv. Atmos. Sci.*, **31**(4), 916–925, doi: 10.1007/s00376-013-3174-0.

1. Introduction

It is well established that the El Niño–Southern Oscillation (ENSO) is the most prominent climate mode of interannual variability in the coupled ocean–atmosphere system. El Niño/La Niña can influence not only tropical regions by causing variation of the Walker circulation, but also further influence extratropical regions (e.g., Klein et al., 1999; Alexander et al., 2002). During El Niño/La Niña mature phases in winter, diabatic heating anomalies over the equatorial central Pacific (CP) can excite the Pacific North American (PNA) pattern (Wallace and Gutzler, 1981) in the Northern Hemisphere and the Pacific South American (PSA) pattern (Robertson and Mechoso, 2003) in the Southern Hemisphere. Besides the atmospheric diabatic heating anomaly over the CP, other diabatic heating anomalies also appear in the tropical Indo-western Pacific (IWP) and the tropical western Indian Ocean (WIO) during El Niño/La Niña mature phases.

Huang (1986) theoretically and numerically investigated the response pattern over middle and high latitudes to the heat source anomaly in low latitudes in winter. In boreal winter, El Niño/La Niña could further influence East Asian precipitation and the winter monsoon system through an anticyclonic circulation anomaly in the lower troposphere (Horel and Wallace, 1981; Wang et al., 1999; Lau and Nath, 2000; Wang and Weisberg, 2000; Wang et al., 2000; Alexander et al., 2002; Wang and Zhang, 2002; Lau et al., 2004; Lau and Nath, 2006). Indeed, it has been demonstrated that oceanic forcing from the tropical eastern Pacific can instigate a low-level anticyclone (Weisberg and Wang, 1997), and the associated air–sea interaction is crucial for rainfall anomalies over East Asia (Wu et al., 2009; Lu et al., 2011). Besides, ENSO events could also impact on the patterns of anomalous temperature and rainfall over East Asia throughout the developing, mature and decaying phases of ENSO via the impact on the East Asian Monsoon system (Zhou et al., 2011). ENSO events play a major role in the summers that follow their ma-

* Corresponding author: WANG Hai
Email: wanghai@ouc.edu.cn

© Institute of Atmospheric Physics/Chinese Academy of Sciences, and Science Press and Springer-Verlag Berlin Heidelberg 2014

ture phases. Over the western North Pacific, a teleconnection pattern named the Pacific–Japan (PJ) pattern was found in summer by Nitta (1987). Under the summer monsoon system, the ENSO-related diabatic heating anomaly center over the Philippines induces a meridional PJ pattern in the lower troposphere, which can then further influence the rainfall and corresponding temperature over Northeast Asia through the baiu/mei-yu front (Kosaka and Nakamura, 2006, 2010a, 2010b).

The aforementioned studies regarding the effect of El Niño/La Niña on East Asian atmospheric circulation were limited to the lower troposphere in both winter and summer. Based on observational data and a simple atmospheric model experiment, Zheng et al. (2013) presented the existence of a new teleconnection pattern induced by a rainfall anomaly in the IWP that emits from the IWP toward East Asia in the upper troposphere during boreal winter: the so-called Indo-western Pacific and East Asia (IWPEA) pattern. This newly defined wave train pattern is induced by the Indo-western Pacific dipole (IWPD) mode of the rainfall anomaly, which shows a similar pattern to the Indian Ocean dipole (IOD) mode (Saji et al., 1999). The simultaneous correlations between the IWPD and Niño3.4 index and between the IWPD and IOD index are 0.87 and 0.68, respectively. Hence, the IWPD is closely related to the IOD events that occur concomitantly with ENSO, and the IWPEA pattern is induced by the joint effect of the IOD and the ENSO event. It has also been shown, by using a simple two-layer atmospheric circulation model, that the heating source is the key factor for the IWPEA pattern, and the background mean flow may also have an influence on the teleconnection pattern (Zheng et al., 2013).

Therefore, during the development phase of ENSO and the IOD, the SST pattern over tropical Indo-Pacific regions will lead to a tropical rainfall anomaly pattern in the following winter. The corresponding diabatic heating anomaly over the CP can excite the PNA and northwestern Pacific anticyclone (NWPA) patterns, and the rainfall anomaly over the IWP and WIO can induce the IWPEA pattern in the upper troposphere (Lu et al., 2011; Zheng et al., 2013; Wang et al., 2013). The question is: can these patterns be simulated by Atmospheric Model Intercomparison Project (AMIP) models from phase five of the Coupled Model Intercomparison Project (CMIP5)? If they can, are there any differences between model simulations and observations? What determines the extra-tropical atmospheric response to El Niño/La Niña? The purpose of the present paper is to answer these questions. The analysis will also help to improve these models in the future.

The paper is organized as follows. Section 2 provides a brief introduction to the data and methods used. Section 3 assesses the simulated rainfall anomaly in the tropical Indo-Pacific regions. Section 4 describes the relationship between Northern Hemisphere atmospheric circulation and the tropical Indo-Pacific rainfall anomaly and examines the differences between model simulations and observations. And finally, section 5 presents a summary and discussion.

2. Data and methods

The data used in this study include the observations and outputs of 11 CMIP5/AMIP models (listed in Table 1). There are many experiments in CMIP5 (Taylor et al., 2012), but here we use the AMIP experiment that is the standard experimental protocol for CMIP5 and provides a community-based infrastructure in support of climate model diagnosis, validation and intercomparison. The AMIP experiment itself is simple by design: it is constrained by realistic SST from 1979 to 2008, with a comprehensive set of fields saved for diagnostic research. It shows the atmospheric circulation responses to the realistic SST, which did not include any errors from the SST differences in coupled climate models of CMIP5. For each model only one member ("r1i1p1") run is used in this study.

To compare the model simulations with the observation, we also analyze various observational and reanalysis datasets. The observed rainfall data are from the Climate Prediction Center (CPC) Merged Analysis of Precipitation (CMAP) (Xie and Arkin, 1996) from 1979 to 2008. The SST dataset is from the monthly National Oceanic and At-

Table 1. The CMIP5/AMIP models used in this study.

Model name	Institute/country	References
BCC-CSM1.1	Beijing Climate Center (BCC), China Meteorological Administration (China)	Wu, 2012
CCSM4	National Center for Climate Research (USA)	Gent et al., 2011
CNRM-CM5	Centre National de Researchss Meteorologiques (France)	Voldoire et al., 2013
FGOALS-g2	Institute of Atmospheric Physics, Chinese Academy of Science (China)	Li et al., 2013
FGOALS-s2	Institute of Atmospheric Physics, Chinese Academy of Science (China)	Bao et al., 2013
GFDL-CM3	Geophysical Fluid Dynamic Laboratory (USA)	Donner et al., 2011
GFDL-HIRAM-C180	Geophysical Fluid Dynamic Laboratory (USA)	Anderson et al., 2004
MIROC5	University of Tokyo, Atmosphere and Ocean Research Institute, National Institute for Environmental Studies, and Japan Agency for Marine-Earth Science and Technology (Japan)	Watanabe et al., 2010
MPI-ESM-LR	Max Planck Institute for Meteorology (German)	Raddatz et al., 2007
MRI-CGCM3	Meteorology Research Institute (Japan)	Yukimoto et al., 2012
NorESM1-M	Norwegian Climate Center (Norway)	Bentsen et al., 2012

mospheric Administration Extended Reconstructed SST V3b (ERSST V3b) (Smith et al., 2008). The atmospheric data used in this study are from the National Centers for Environmental Prediction/National Center for Atmospheric Research (NCEP/NCAR) reanalysis dataset (Kalnay et al., 1996). The climatology is based on the time period of 1979–2008 corresponding to the model outputs.

For comparing similarities and differences between the different CMIP5/AMIP models and the observed results, we have interpolated all model simulations to a $2.5^\circ \times 2.5^\circ$ horizontal resolution based on the NCEP/NCAR data. First, we examine the climatology and interannual variability of the tropical rainfall for the period 1979–2008. Following previous studies (e.g., Zheng et al., 2013), three rainfall indexes are defined in assessing the effect of the simulations. Regression analysis shows the impact of the tropical rainfall anomaly on the Northern Hemisphere atmospheric circulation anomaly. The observed Niño3.4 index is used as a unified indicator in the regression analysis. To focus on the interannual variability, the linear trend has been removed from the original data.

According to Takaya and Nakamura (2001), the wave-activity flux [Eq. (1)] is parallel to the local three-dimensional group velocity of Rossby waves, and hence suitable for a snapshot diagnosis of the three-dimensional propagation of wave packets of migratory and stationary eddies on a zonally-varying basic flow.

$$\boldsymbol{W} = \frac{P}{2|\boldsymbol{U}|}\begin{pmatrix} U(\psi_x'^2 - \psi'\psi_{xx}') + V(\psi_x'\psi_y' - \psi'\psi_{xy}') \\ U(\psi_x'\psi_y' - \psi'\psi_{xy}') + V(\psi_y'^2 - \psi'\psi_{yy}') \end{pmatrix}. \quad (1)$$

U and V in Eq. (1) represent the monthly mean zonal and meridional wind, respectively; P is the pressure normalized by 1000 hPa; and ψ' denotes the monthly anomalous stream function at the 200 hPa level, with the subscripts x and y referring to their partial differentials in the zonal and meridional direction, respectively.

3. Simulated tropical Indo-Pacific rainfall

The AMIP experiments used in this study are constrained by realistic SST from 1979 to 2008. In order to examine the reproducibility of climatological mean and interannual variation of the rainfall response to the SST forcing in the AMIP experiments, we calculated the climatological mean and interannual standard deviation (ISD) of the tropical rainfall in December–February (DJF) compared with the observed results. Figure 1a illustrates that all of the models simulate well the positions of the climatological maximum rainfall, which are located in the Intertropical Convergence Zone (ITCZ) and South Pacific Convergence Zone (SPCZ). Figure 1b shows that the rainfall ISD is of the same magnitude compared with the climatological rainfall. It indicates that the simulated ISD of tropical rainfall in the multi-model ensemble (MME) can capture the basic features in the observation (the maximum center locates near the dateline). However, the MME result shows larger rainfall ISD over the IWP (20°S–20°N, 110°–150°E) and the entire South Indian Ocean (0°–20°S). Despite the differences of intensity in the simulated rainfall ISD, it still locates where the climatological maximum rainfall band lies, and this will lead to significant rainfall interannual variation that may have an influence on the atmospheric circulation through the release of latent heat of condensation.

The ISD of the rainfall anomaly in the CP (5°S–5°N,

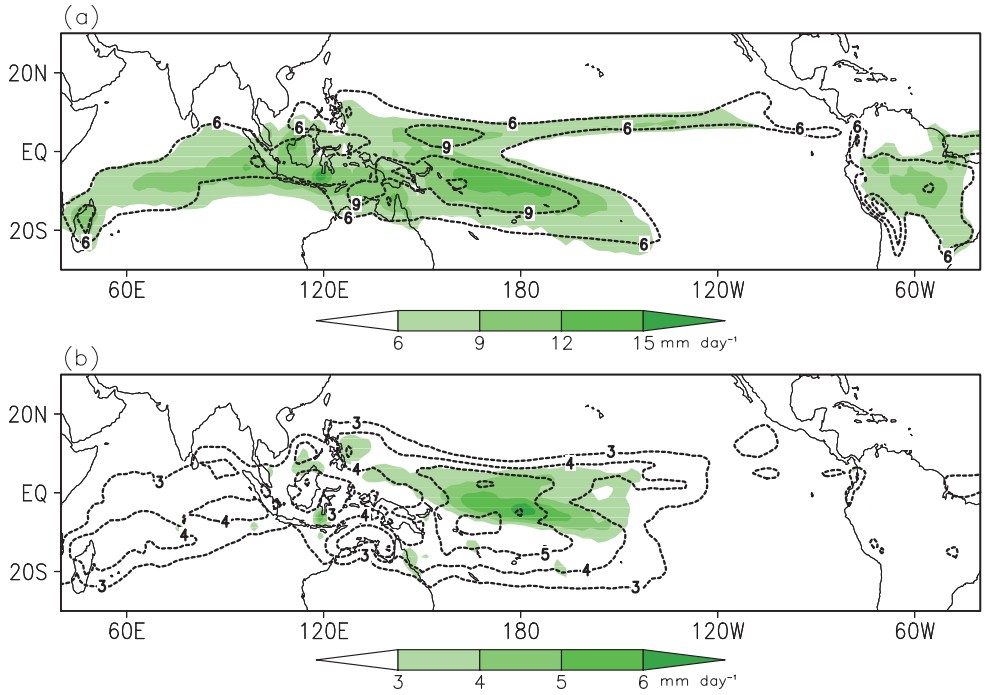

Fig. 1. (a) Climatological mean rainfall and (b) interannual standard deviation of rainfall anomalies in DJF from 1979 to 2008 in the observation (shading) and MME mean (dashed contour).

175°E–135°W) and the IWPD index [the standard deviation of the rainfall anomaly differences between the IWP (20°S–20°N, 110°–150°E) and WIO (10°S–10°N, 45°–75°E)] during 1979–2008 are shown in Table 2. The simulated ISD of the rainfall is quite different among these models. Over the CP, seven out of the 11 models simulate a stronger rainfall ISD compared to the observed result. Over the IWP and WIO, most of the simulated amplitude is much weaker than the observation except for the MRI-CGCM3 model in the IWP and the MPI-ESM-LR, CNRM-CM5, GFDL-CM3 and FGOALS-s2 models in the WIO. All the IWPD indexes in the models are smaller than in the observation.

Figure 2a shows that the simulated CP rainfall anomaly corresponds to the observation well with a correlation coefficient of 0.99. The rainfall index can clearly depict El Niño events: 1982/83, 1986/87, 1991/92, 1994/95, 1997/98 2002/03, 2006/07; and La Niña events: 1984/85, 1988/89, 1995/96, 1998/2000, 2005/06 and 2007/08. There are some differences in amplitude between the observation and simulations. The simulated rainfall anomaly indexes in the IWP (Fig. 2b) and in the WIO (Fig. 2c) are also close to the observations (0.85 for IWP and 0.61 for WIO), but the differences are larger than in the CP.

In summary, the 11 CMIP5/AMIP models perform well in simulating the climatological mean and variation of the tropical rainfall, especially in the CP. But how will the rainfall anomaly in the tropical regions influence the Northern Hemisphere atmospheric circulation? Do these models have the ability to reproduce the teleconnection patterns? We attempt to address these questions in the next section.

4. Relationship between the Northern Hemisphere atmospheric circulation anomaly and tropical Indo-Pacific rainfall anomaly

Although the SST anomaly is the same in different models, the tropical rainfall anomalies are different because of the different convection and coupled ocean–atmosphere parameterization schemes and other settings among the models. The different tropical rainfall anomalies will lead to different diabatic heating sources in the atmosphere, and then cause the different response in the atmosphere. In order to prove that the different response of the atmospheric circulation to ENSO is dependent on the intensity of the tropical rainfall anomalies in the different models, in this section we analyze the relationship between the Northern Hemisphere atmospheric circulation anomaly and tropical Indo-Pacific rainfall anomaly by dividing the models into different groups according to their simulation ability of the tropical rainfall variation over different regions.

Table 2. The interannual standard deviation (ISD; units: mm d^{-1}) of the rainfall anomaly over the CP and the IWPD index in the observation and 11 CMIP5/AMIP outputs (bold values indicate those models in Group_1 and Group_3).

Model	CP	IWPD
(a) CMAP (observation)	2.96	2.04
(b) MPI-ESM-LR	**4.05**	**1.92**
(c) FGOALS-g2	**3.38**	**1.55**
(d) CCSM4	**3.24**	1.07
(e) CNRM-CM5	**3.20**	**1.64**
(f) GFDL-CM3	**3.19**	1.28
(g) NorESM1-M	**3.10**	1.13
(h) MRI-CGCM3	**3.09**	**1.81**
(i) FGOALS-s2	2.95	**1.41**
(j) MIROC5	2.37	1.21
(k) BCC-CSM1.1	2.13	1.23
(l) GFDL-HIRAM-C180	2.04	0.73

4.1. *CP rainfall anomaly and corresponding teleconnection patterns*

The intensity of the PNA teleconnection pattern is related to tropical central-eastern Pacific rainfall (Lee et al., 2009). Based on their ability in simulating the CP rainfall variation, the 11 CMIP5/AMIP models are divided into two groups. The models in Group_1 have a stronger climatological (4.0 mm d^{-1} in Group_1 ensemble and 2.8 mm d^{-1} in Group_2 ensemble) and ISD (listed in Table 2; Group_1 includes those models with larger CP rainfall ISD than the observation of 2.96 mm d^{-1}) of rainfall over the CP: MPI-ESM-LR, FGOALS-g2, CCSM4, CNRM-CM5, GFDL-CM3, NorESM1-M, and MRI-CGCM3; whereas the rest (Group_2) have a weaker rainfall ISD: FGOALS-s2, MIROC5, BCC-CSM1.1, and GFDL-HIRAM-C180. The climatological rainfall and the ISD over the CP are positively correlated with each other between the two model group ensembles. To address the Northern Hemisphere atmospheric circulation response to the CP rainfall anomaly during boreal winter, a regression map of the DJF 200-hPa geopotential height anomaly (H200A) onto DJF Niño3.4 index was calculated (Fig. 3). The simulated PNA patterns are well captured in both groups (Figs. 3b and c) in comparison with the observation (Fig. 3a). The PNA pattern shows negative anomalies of geopotential height over the Northeast Pacific, positive anomalies over Canada, and negative anomalies over the southeastern United States (Horel and Wallace, 1981). As shown in Fig. 3, the ray path of the PNA wave train connecting the anomalous centers is directed poleward first, then curves eastward, and is finally directed back equatorward (Hoskins and Karoly, 1981). Due to the strong CP rainfall simulated in the Group_1 models, the simulated PNA pattern in the Group_1 models is stronger than that of the Group_2 models, although the SST anomaly is the same in the 11 CMIP5/AMIP models.

Further evidence to support the idea that the intensity of the PNA pattern is correlated with the CP rainfall variation is shown in the scatter diagram in Fig. 3d. It shows the relationship between the maximum value of the 200-hPa geopotential height anomaly ISD over the negative center related with the PNA pattern (30°–60°N, 180°–120°W) and the CP rainfall ISD. The result indicates that the intensity of the PNA pattern intensifies with the CP rainfall variation at the correlation coefficient 0.51, and through the scatter we can dis-

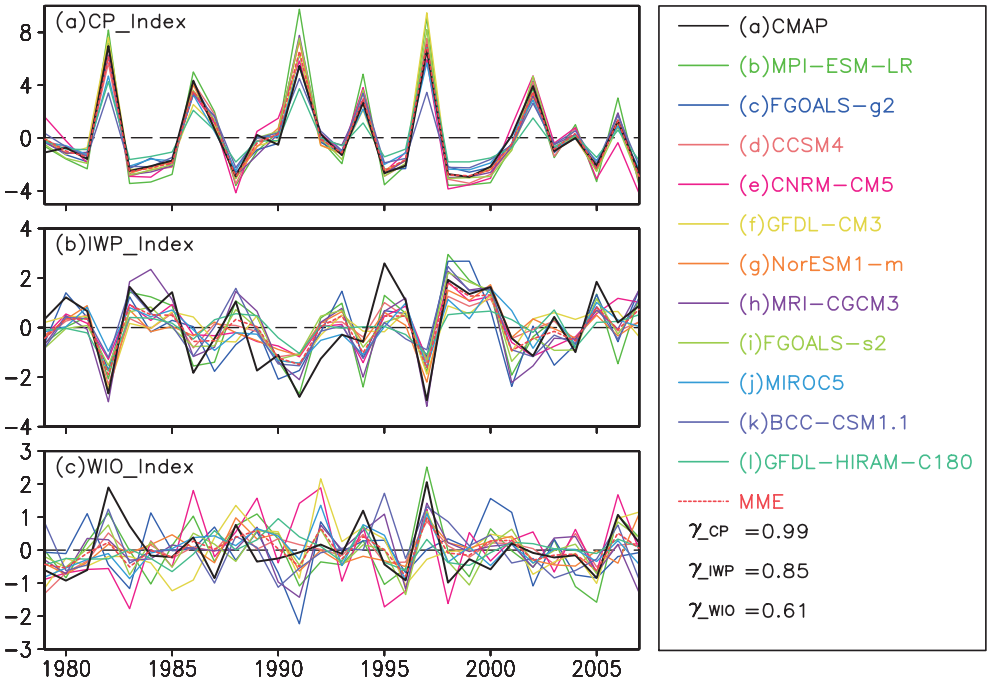

Fig. 2. Time series of rainfall anomaly (units: mm d^{-1}) over the (a) CP, (b) IWP, and (c) WIO in DJF and the correlation coefficients between the observation and the MME. Years represent the average of the December in that year and the following January and February.

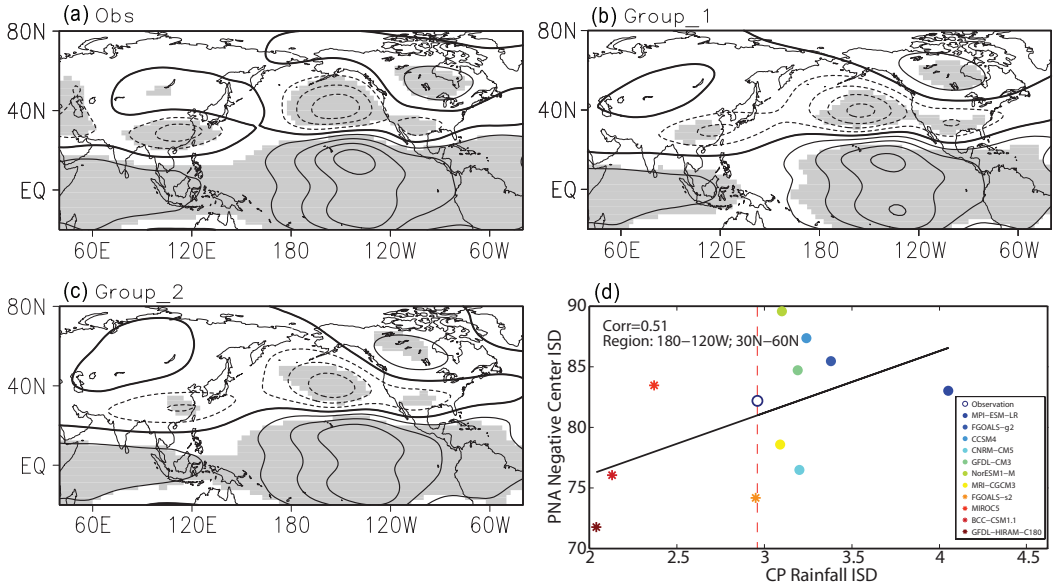

Fig. 3. Regressions of the DJF 200-hPa geopotential height anomaly on the DJF Niño3.4 index from 1979 to 2008 (contours at 10 m intervals; 0 is thickened) in the (a) observation (b, c) two groups of CMIP5/AMIP models. The grey shading denotes the 90% confidence level for H200A. (d) Scatter diagram (*y*-axis units: m; *x*-axis units: mm d^{-1}) of the intensity of the PNA negative center [*y*-axis represents the maximum value of the 200-hPa geopotential height anomaly ISD over (30°–60°N, 180°–120°W)] and the CP rainfall ISD. The red dashed line in (d) indicates the criterion of the grouping.

tinguish that most of the Group_1 models simulate the PNA pattern stronger than those in Group_2, except for some bias in models MRI-CGCM3, CNRM-CM5 and MIROC5. Concerning the model bias due to some unclear settings, these results are robust enough to identify that the intensity of the PNA pattern is dependent on the atmospheric diabatic heating (rainfall) anomaly over the CP.

Another important feature regarding the ENSO's influence on atmospheric circulation is the anomalous anticyclone (cyclone) in the Northwestern Pacific (east of the Philippines

in the lower troposphere) during El Niño/La Niña (Wang et al., 1999; Wang and Weisberg, 2000; Wang et al., 2000; Wu et al., 2010a). The atmosphere–ocean coupled Rossby wave induced by the SST anomaly in the eastern equatorial Pacific propagates westward to the western Pacific in the lower troposphere and then leads to the decrease (increase) of the local SST. Through the local ocean–atmosphere interactions, the anomalous anticyclone (cyclone) is formed (Wang et al., 1999; Wang and Weisberg, 2000; Wang et al., 2000; Wu et al., 2010b). In the above-mentioned studies, the main concern is its relationship with the SST anomaly in either the tropical Eastern Pacific or Indian Ocean, or the local SST anomaly condition. Besides, Zhou et al. (2009) showed that, in the CMIP3/AMIP models, the prominent feature of the first leading mode of Asian–Australian monsoon variability includes the anticyclonic anomaly over the western North Pacific during DJF, and the strength of it in the AMIP models is also associated with deficiencies in the simulated intensities of the rainfall anomaly. Our focus, however, is whether it is dependent on the rainfall anomaly over the CP. In order to check whether this feature is shown in the 11 CMIP5/AMIP models, we calculated the regressions of 850-hPa wind and geopotential height anomalies onto the DJF Niño3.4 index (Fig. 4). All of the CMIP5/AMIP models can reproduce the anomalous anticyclone east of the Philippines in the lower troposphere. In the Group_1 models (Fig. 4b), the simulated anomalous anticyclone is much stronger than that in the observation (Fig. 4a), as well as in the Group_2 models (Fig. 4c), due to the intensified rainfall variation over the CP.

The relationship between the CP rainfall ISD and the maximum 850-hPa geopotential height anomaly ISD [over (0°–20°N, 115°–145°E)] also illustrates that the intensity of the intensity of the NWPA varies with the CP rainfall ISD as well (0.62 in Fig. 4d). The scatter in Fig. 4d indicates that all the Group_2 models show a weaker NWPA than the observation and those models in Group_1, except for the FGOALS-s2 model. This result also backs up the implication from the regression analysis in the above two groups that the CP rainfall anomaly is a key factor affecting the wintertime anomalous anticyclone or cyclone in the northwestern Pacific driven by remote ENSO forcing.

In general, the CMIP5/AMIP experiments simulate the rainfall variation over the CP well. It is found, through the SST anomaly being the same in the 11 CMIP5/AMIP models, that the intensity of the PNA pattern and the lower tropospheric atmospheric circulation anomaly east of the Philippines correlates well with the intensity of the rainfall anomaly over the CP. This illustrates that the intensity of the diabatic heating anomaly over the CP can affect the intensity of the PNA pattern and the wintertime anomalous anticyclone or

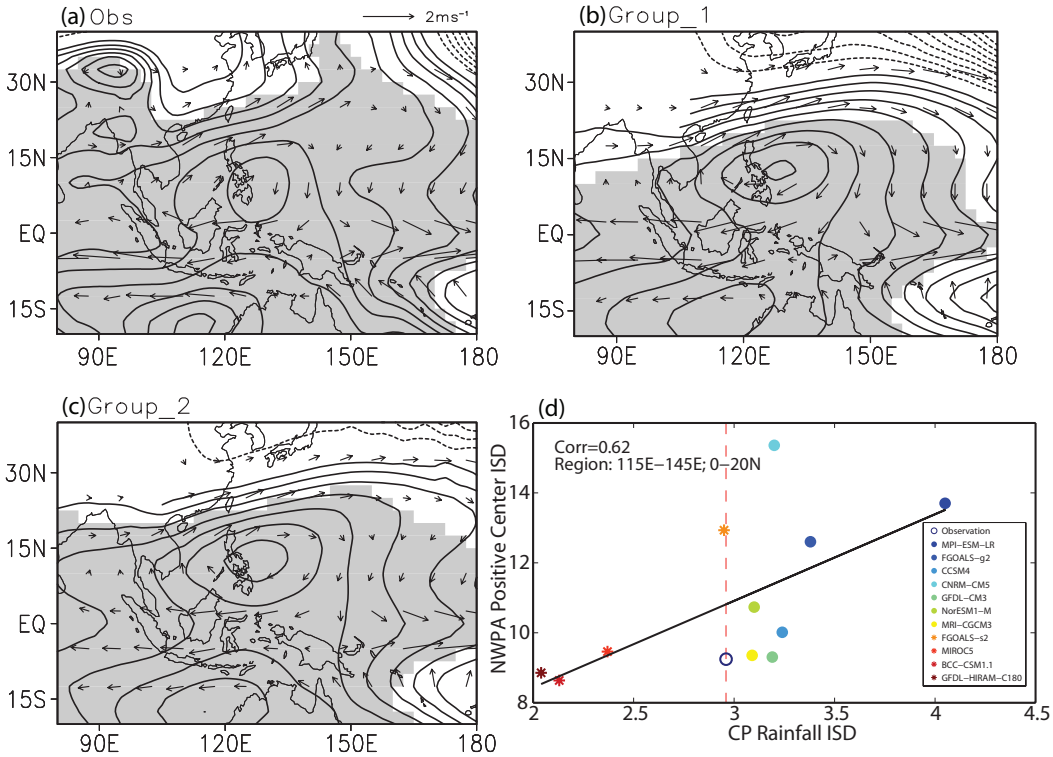

Fig. 4. Regressions of the DJF 850-hPa wind anomaly (vectors) and geopotential height anomaly (contours at 1-m intervals; 0 is omitted) on DJF Niño3.4 index from 1979 to 2008 in the (a) observation and (b, c) two groups of CMIP5/AMIP models. The grey shading denotes the 90% confidence level for H850A. (d) Scatter diagram (*y*-axis units: m; *x*-axis units: mm d^{-1}) of the intensity of the NWPA positive center [*y*-axis represents the maximum value of the 850-hPa geopotential height anomaly ISD over (0°–20°N, 115°E–145°W)] and the CP rainfall ISD. The red dashed line in (d) indicates the criterion of the grouping.

cyclone in the northwestern Pacific.

4.2. *IWP and WIO rainfall anomaly and the corresponding IWPEA pattern*

Besides the PNA pattern, from Figs. 3a–c we can also address the influence of ENSO on East Asian upper tropospheric atmospheric circulation. Corresponding to the CP rainfall anomaly induced by ENSO, the anomalous Walker circulation will lead to a west–east dipole pattern of the boreal winter rainfall over the tropical IWP and WIO (IWPD), and induce the IWPEA pattern over East Asia (Zheng et al., 2013). In the CMIP5/AMIP models, it can be found that the East Asian atmospheric responses to ENSO in both Group_1 and Group_2 are a little weaker than in the observation (Figs. 3a–c). This is because the rainfall anomaly over the IWP and WIO (Figs. 2b and c) and the IWPD (Table 2) indexes are smaller than in the observation. A multiple linear regression analysis shows that the rainfall anomalies over both the IWP and WIO make a contribution to the wave train pattern. Meanwhile the regression of the 200-hPa geopotential height anomaly onto the IWP rainfall anomaly is more similar to the IWPEA pattern, which is a regression onto the Niño3.4 index as a unified indicator, compared with the results of the regression onto the WIO rainfall anomaly. Therefore, we take the IWP and WIO rainfall variation jointly into consideration in the following analysis. The models are categorized into another two groups based on the IWPD indexes. Models in Group_3 (IWPD index>1.3 mm d^{-1}: MPI-ESM-LR, MRI-CGCM3, CNRM-CM5, FGOALS-g2 and FGOALS-s2) simulate the tropical rainfall variation closer to the observation and larger than in Group_4 (the rest of the models).

In order to verify the simulation of the interannual variation of the upper tropospheric atmospheric circulation in the 11 CMIP5/AMIP models, regression analysis of DJF H200A and horizontal wave-activity flux [defined in Eq. (1)] onto the DJF Niño3.4 index is applied in Fig. 5. The horizontal wave-activity flux is suitable for a snapshot analysis of stationary or migratory eddies on a zonally-varying basic flow (Takaya and Nakamura, 2001) and presents the propagating low-frequency perturbation energy. Figure 5 examines the relative importance of the anomalous rainfall over the tropical IWP and WIO in the IWPEA wave train and shows the existence of the IWPEA wave train pattern in the 11 CMIP5/AMIP models. Comparing Figs. 5a, b and c, it is

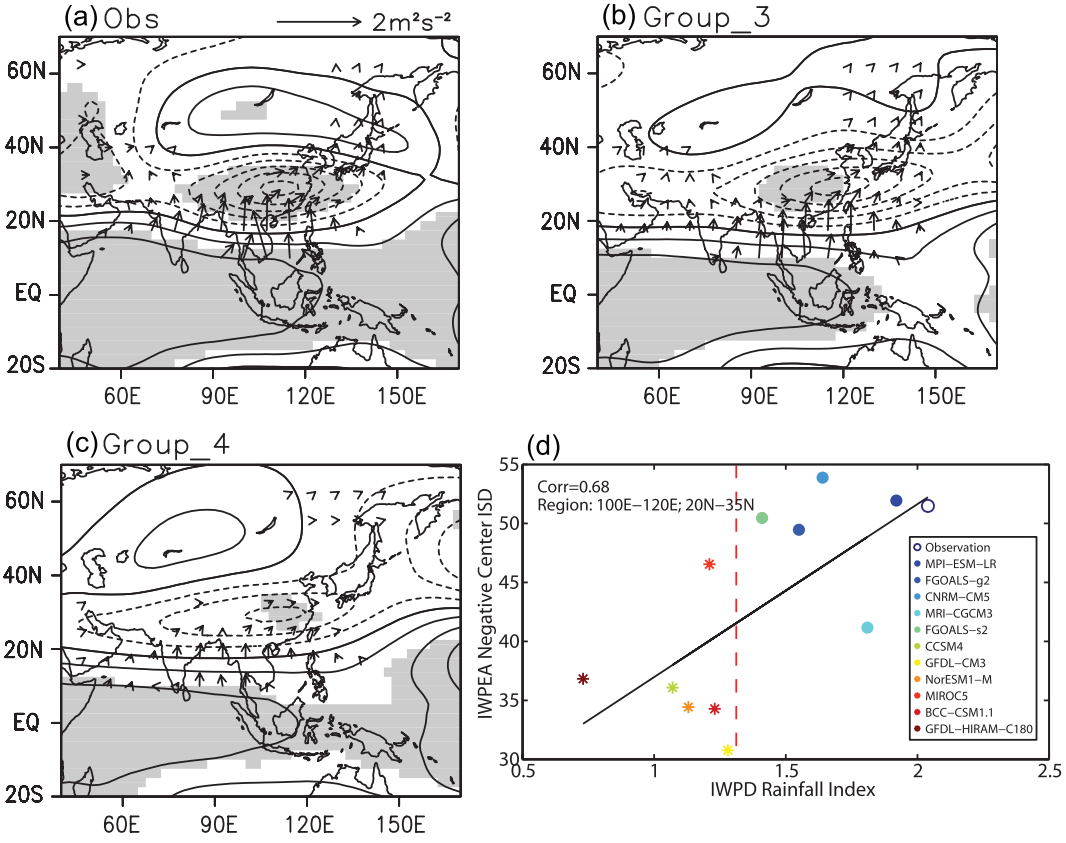

Fig. 5. Regression of the DJF 200-hPa level geopotential height anomaly (contours at 5-m intervals; 0 is thickened) and wave-activity flux [vectors; only shown are the $y > 0$ m^2 s^{-2} meridional components, with the scalar in the top-right corner of (a)] on DJF Niño3.4 index from 1979 to 2008 in the (a) observation and (b, c) two groups of CMIP5/AMIP models. The grey shading denotes the 90% confidence level for regressed H200A. (d) Scatter diagram (*y*-axis units: m; *x*-axis units: mm d^{-1}) of the intensity of the IWPEA negative center [*y*-axis represents the maximum value of the 200-hPa geopotential height anomaly ISD over (20°–35°N, 100°–120°E)] and the IWPD rainfall index. The red dashed line in (d) indicates the criterion of the grouping.

found that both groups (Group_3 and Group_4) simulate well the IWPEA wave train from the tropical IWP toward Northeast Asia. However, the amplitude of the wave train and wave-activity flux in Figs. 5b and c are smaller than in Fig. 5a (observation), and this is because the IWPD indexes in the 11 models are smaller than in the observation (Table 2). In particular, as the IWPD index is larger in Group_3 than in Group_4, the amplitude of the wave train and wave-activity flux are larger in Group_3 than in Group_4 (Figs. 5b and c).

For the IWPEA pattern, we also analyzed the relationship between the maximum value of the 200-hPa geopotential height anomaly ISD corresponding to the IWPEA pattern [over (20°–35°N, 100°–120°E)] and the IWPD rainfall index in each of the models, as shown in Fig. 5d. The ISD of the IWPEA negative center is well correlated with the variation of the IWPD index at 0.68. Due to the weaker IWPD index in the models, nearly all the models show a weaker intensity of the IWPEA pattern, especially in Group_4; and furthermore, most of the models in Group_4 show much weaker IWPEA intensity than those in Group_3.

Based on the above analysis, both the observational data and the models forced by realistic SST in general jointly verify the existence of the IWPEA pattern in the upper troposphere. The difference in the anomalous heating released by the anomalous rainfall over the IWP and WIO is the key factor in determining the existence and intensity of the teleconnection pattern. As the IWPD indexes are weaker in all the CMIP5/AMIP models, the simulated intensity of the IWPEA pattern is weaker than that in the observation. In MPI-ESM-LR, MRI-CGCM3, CNRM-CM5, FGOALS-g2 and FGOALS-s2 (five models of Group_3), the simulated IWPEA pattern is more similar to that in the observation, and this is because the IWPD indexes are closer to the observation.

5. Summary and discussion

In this study, the interannual variability of the rainfall anomaly in the tropical Pacific and Indian Ocean and its influence on Northern Hemisphere atmospheric circulation was analyzed based on observations and CMIP5/AMIP experiments forced by realistic SST. The climatological mean of the rainfall in the simulated situations shows that the CMIP5/AMIP experiments can capture the basic features of the rainfall patterns over the tropics, while the ISD of the rainfall anomaly shows some differences in intensity. It is found that the CMIP5/AMIP simulations can reproduce the anomalous rainfall signal well, especially over the CP and IWP. In order to verify the impact of the rainfall anomaly over tropical Indo-Pacific regions on Northern Hemisphere atmospheric circulation, regressions of the H200A and wave-activity flux based on the Niño3.4 index were conducted. The results show that a stronger rainfall ISD over the CP will lead to a stronger PNA and NWPA pattern.

For the IWP and WIO, the newly defined IWPD index is weaker in the 11 CMIP5/AMIP models and therefore leads to a weaker wave train pattern from the IWP toward East Asia. The intensity of the positive–negative H200A and northward wave-activity fluxes in different models and groups show that the differences of the diabatic heating anomaly between the IWP and WIO induced by the tropical rainfall anomaly there is the key factor regulating the IWPEA pattern. For the IWPEA pattern, some CMIP5/AMIP models, such as MPI-ESM-LR, MRI-CGCM3, CNRM-CM5, FGOALS-g2 and FGOALS-s2, are able to simulate it well, because they can reproduce the IWPD pattern of the rainfall anomaly closer to the observation.

In this paper, the key point was to detect the relationship between the intensity of the tropical rainfall anomaly and the atmospheric teleconnection pattern response when the SST anomaly was the same in different CMIP5/AMIP simulations. The CMIP5/AMIP experiment is designed to be forced by realistic SST, and thus mainly focuses on atmospheric internal variation and its responses to observed SST without the ocean–atmosphere interaction processes like those in the coupled models. Hence, there are significant differences in the convection and coupled ocean–atmosphere parameterization schemes in different models. These differences in model design will lead to different tropical responses in different models, as well as variation in the atmospheric background field, such as the simulation of the monsoon system. Therefore, the different tropical rainfall anomalies will lead to different diabatic heating sources in the atmosphere and subsequently cause different responses in the atmosphere. These aspects need to be examined in further work.

Acknowledgements. The authors thank Prof. Shang-Ping XIE and Chun-Zai WANG for their constructive comments and suggestions. This work is supported by the Ministry of Science and Technology of China (National Basic Research Program of China; Grant No. 2012CB955602) and the National Natural Science Foundation of China (Grant Nos. 41176006 and 41221063). We acknowledge the World Climate Research Programme's Working Group on Coupled Modeling, which is responsible for CMIP5, and we thank the climate modeling groups (listed in Table 1) for producing and making available their model outputs.

REFERENCES

Alexander, M. A., I. Blade, M. Newman, J. R. Lanzante, N. C. Lau, and J. D. Scott, 2002: The atmospheric bridge: The influence of ENSO teleconnections on air-sea interaction over the global oceans. *J. Climate*, **15**, 2205–2231.

Anderson, J. L., and Coauthors, 2004: The new GFDL global atmosphere and land model AM2-LM2: Evaluation with prescribed SST simulations. *J. Climate*, **17**, 4641–4673.

Bao, Q., and Coauthors, 2013: The Flexible Global Ocean-Atmosphere-Land System model, Spectral Version 2: FGOALS-s2, *Adv. Atm. Sci.* **30**(3), 561–576, doi: 10.1007/s00376-012-2113-9.

Bentsen, M., and Coauthors, 2012: The Norwegian earth system model, NorESM1-M-Part 1: Description and basic evaluation. *Geoscientific Model Development Discussions*, **5**, 2843–2931.

Donner, L. J., and Coauthors, 2011: The Dynamical core, physical parameterizations, and basic simulation characteristics of the atmospheric component AM3 of the GFDL Global Coupled Model CM3. *J. Climate*, **24**(13), 3484–3519.

Gent, P. R., and Coauthors, 2011: The Community Climate System Model version 4. *J. Climate*, **24**, 4973-4991, doi: 10.1175/2011JCLI4083.1

Horel, J. D., and J. M. Wallace, 1981: Planetary-scale atmospheric phenomena associated with the Southern Oscillation. *Mon. Wea. Rev.*, **109**, 813–829.

Hoskins, B. J., and D. J. Karoly, 1981: The steady linear response of a spherical atmosphere to thermal and orographic forcing. *J. Atmos. Sci.*, **38**(6), 1179–1196.

Huang, R. H., 1986: Physical mechanism of influence of heat source anomaly over low latitudes on general circulation over Northern Hemisphere in winter. *Scientia Sinica-Series B*, **29**(1), 91–103.

Kalnay, E., and Coauthors, 1996: The NCEP/NCAR 40–year reanalysis project. *Bull. Amer. Meteor. Soc.*, **77**, 437–471.

Klein, S. A., B. J. Sode, and N. C. Lau, 1999: Remote sea surface temperature variations during ENSO: Evidence for a tropical atmospheric bridge. *J. Climate*, **12**, 917–932.

Kosaka, Y., and H. Nakamura, 2006: Structure and dynamics of the summertime Pacific-Japan teleconnection pattern. *Quart. J. Roy. Meteor. Soc.*, **132**, 2009–2030.

Kosaka, Y., and H. Nakamura, 2010a: Mechanisms of meridional teleconnection observed between a summer monsoon system and a subtropical anticyclone. Part I: The Pacific-Japan Pattern. *J. Climate*, **23**, 5085–5108.

Kosaka, Y., and H. Nakamura, 2010b: Mechanisms of meridional teleconnection observed between a summer monsoon system and a subtropical anticyclone. Part II: A global survey. *J. Climate*, **23**, 5109–5125.

Lau, N. C., and M. J. Nath, 2000: Impact of ENSO on the variability of the Asian-Australian monsoons as simulated in GCM experiments. *J. Climate*, **13**, 4287–4309.

Lau, N. C., and M. J. Nath, 2006: ENSO modulation of the interannual and variability of the East Asian monsoon-A model study. *J. Climate*, **19**, 4508–4530.

Lau, N. C., M. J. Nath, and H. Wang, 2004: Simulations by a GFDL GCM of ENSO-related variability of the coupled atmosphere-ocean system in the East Asian monsoon region. *East Asian Monsoon. World Scientific Series on Meteorology of East Asia*, Vol. 2, C. P. Chang. Ed., Singapore, World Scientific, 271–300.

Lee, S. K., C. Z. Wang, and B. E. Mapes, 2009: A simple atmospheric model of the local and teleconnection responses to tropical heating anomalies. *J. Climate*, **22**, 272–284.

Li, L. J., and Coauthors, 2013: The flexible global ocean-atmosphere-land system model, Grid-point Version 2: FGOALS-g2. *Adv. Atmos. Sci.* **30**(3), 543–560, doi: 10.1007/s00376-012-2140-6.

Lu, J., M. Zhang., B. Cash, and S. Li, 2011: Oceanic forcing for the East Asian rainfall in pace-making AGCM experiments. *Geophys. Res. Lett*., **38**(L12702), doi: 10.1029/2011GL047814.

Nitta, T., 1987: Convective activities in the tropical western Pacific and their impact on the northern hemisphere summer circulation. *J. Meteor. Soc. Japan*, **65**, 373–390.

Raddatz, T., and Coauthors, 2007: Will the tropical land biosphere dominate the climate–carbon cycle feedback during the twenty-first century? *Clim. Dyn.*, **29**(6): 565–574.

Robertson, A. W., and C. R. Mechoso, 2003: Circulation regimes and low-frequency oscillations in the South Pacific sector. *Mon. Wea. Rev.*, **131**, 1566–1576.

Saji, N. H., B. N. Goswami, P. N. Vinayachandran, and T. Yamagata, 1999: A dipole mode in the tropical Indian Ocean. *Nature*, **401**, 360–363.

Smith, T. M., R. W. Reynolds, T. C. Peterson, and J. Lawrimore, 2008: Improvements to NOAA's historical merged land-ocean surface temperature analysis (1880–2006). *J. Climate*, **21**, 2283–2296.

Takaya, K., and H. Nakamura, 2001: A formulation of a phase-independent wave-activity flux for stationary and migratory quasigeostrophic eddies on a zonally varying basic flow. *J. Atmos. Sci.*, **58**, 608–627.

Taylor, K. E., R. J. Stouffer, and G. A. Meehl, 2012: An Overview of CMIP5 and the experiment design. *Bull. Amer. Meteor. Soc.*, **93**, 485–498.

Voldoire, A., and Coauthors, 2013: The CNRM-CM5. 1 global climate model: Description and basic evaluation. *Climate Dyn.*, **40**, 2091-2121.

Wallace, J. M., and D. S. Gutzler, 1981: Teleconnections in the geopotential height field during the Northern Hemisphere winter. *Mon. Wea. Rev.*, **109**, 784–812.

Wang, B., and Q. Zhang, 2002: Pacific-East Asian teleconnection. Part II: How the Philippine Sea anomalous anticyclone is established during El Niño development? *J. Climate*, **15**, 1643–1658.

Wang, B., R. Wu, and X. Fu, 2000: Pacific-East Asian teleconnection: How does ENSO affect East Asian climate? *J. Climate*, **13**, 1517–1536.

Wang, C. Z., and R. H. Weisberg, 2000: The 1997–98 El Niño evolution relative to previous El Niño events. *J. Climate*, **13**, 488–501.

Wang, C. Z., R. H. Weisberg, and J. I. Virmani, 1999: Western Pacific interannual variability associated with the El Niño-Southern Oscillation. *J. Geophys. Res.*, **104**, 5131–5149.

Wang, H., Q. Y. Liu, and J. Zheng, 2013: Formation mechanism for the anomalous anticyclonic circulation over Northeast Asia and the Japan Sea in boreal winter 1997/98 and the spring of 1998. *Journal of Ocean University of China*, **12**(2), 312–317.

Watanabe, and Coauthors, 2010: Improved climate simulation by MIROC5: Mean states, variability, and climate sensitivity. *J. Climate*, **23**, 6312–6335.

Weisberg, R. H., and C. Z. Wang, 1997: A western Pacific oscillator paradigm for the El Niño-Southern Oscillation. *Geophys. Res. Lett.*, **24**, 779–782.

Wu, B., T. J. Zhou, and T. Li, 2009: Seasonally evolving dominant interannual variability modes of East Asian climate. *J. Climate*, **22**(11), 2992–3005.

Wu, B., T. Li, and T. J. Zhou, 2010a: Asymmetry of atmospheric circulation anomalies over the western North Pacific between El Niño and La Niña. *J. Climate*, **23**, 4807–4822.

Wu, B., T. Li, and T. J. Zhou, 2010b: Relative contributions of the Indian Ocean and local SST anomalies to the maintenance of the western North Pacific anomalous anticyclone during El Niño decaying summer. *J. Climate*, **23**, 2974–2986.

Wu, T., 2012: A mass-flux cumulus parameterization scheme for large-scale models: Description and test with observations. *Climate Dyn.*, **38**, 725–744.

Xie, S., and P. A. Arkin, 1996: Analyses of global monthly precipitation using gauge observations, satellites estimates, and numerical model predictions. *J. Climate*, **9**, 840–858.

Yukimoto, S., Y. Adachi, and M. Hosaka, 2012: A new global climate model of the Meteorological Research Institute: MRI-CGCM3: Model description and basic performance. *J. Meteor. Soc. Japan*, **90**A, 23–64.

Zheng, J., Q. Y. Liu, C. Z. Wang, and X. T. Zheng, 2013: Impact of heating anomalies associated with rainfall variations over the indo-western Pacific on Asian atmospheric circulation in winter. *Climate Dyn.*, **40**, 2023–2033.

Zhou, T. J., B. Wu, and B. Wang, 2009: How well do atmospheric general circulation models capture the leading modes of the interannual variability of the Asian-Australian Monsoon? *J. Climate*, **22**, 1159–1173.

Zhou, T. J., H. Hsu, and J. Matsuno, 2011: Summer monsoons in East Asia, Indochina, and the western North Pacific. *The Global Monsoon System: Research and Forecast*. 2nd ed., C. P. Chang et al., Eds., 2011 World Scientific Publishing Co., 43–72.